Eur. Phys. J. Plus (2017) **132**: 245
DOI 10.1140/epjp/i2017-11503-0

THE EUROPEAN PHYSICAL JOURNAL PLUS

Regular Article

# Aerosol concentration measurements and correlations with air mass trajectories at the Pierre Auger Observatory

M.I. Micheletti[1,2,a], K. Louedec[3], M. Freire[1], P. Vitale[4,5], and R.D. Piacentini[1,6]

[1] Instituto de Física Rosario (IFIR) CONICET/UNR, Bv. 27 de Febrero 210 bis, Rosario, Argentina
[2] Facultad de Ciencias Bioquímicas y Farmacéuticas, Universidad Nacional de Rosario (UNR), Suipacha 531, Rosario, Argentina
[3] M6 group, 92200 Neuilly-sur-Seine, France
[4] Comisión Nacional de Energía Atómica, Av. del Libertador 8250, Ciudad Autónoma de Buenos Aires, Argentina
[5] Pierre Auger Observatory, Av. San Martín Norte 304 (5613), Malargüe, Argentina
[6] Facultad de Ciencias Exactas, Ingenieria y Agrimensura, UNR, Av. Pellegrini 250, Rosario, Argentina

Received: 20 June 2016 / Revised: 12 April 2017
Published online: 1 June 2017 – 

**Abstract.** Aerosols play an important role in radiative transfer processes involved in different fields of study. In particular, their influence is crucial in the attenuation of light at astronomical and astrophysical observatories, and has to be taken into account in light transfer models employed to reconstruct the signals. The Andean Argentinean region is increasingly being considered as a good candidate to host such facilities, as well as the ones for solar-energy resources, and an adequate knowledge of aerosols characteristics there is needed, but it is not always possible due to the vast area involved and the scarce atmospheric data at ground. The aim of this work is to find correlations between aerosol data and particle trajectories that can give an insight into the origin and behaviour of aerosols in this zone and can be employed in situations in which one does not have local aerosol measurements. For this purpose, an aerosol spectrometer and dust monitor (Grimm 1.109) was installed at the Pierre Auger Observatory of ultra-high-energy cosmic rays, to record aerosol concentrations in different size intervals, at surface level. These measurements are analysed and correlated with air mass trajectories obtained from HYSPLIT (NOAA) model calculations. High aerosol concentrations are registered predominantly when air masses have travelled mostly over continental areas, mainly from the NE direction, while low aerosol concentrations are found in correspondence with air masses coming from the Pacific Ocean, from the NW direction. Different size distribution patterns were found for the aerosols depending on their origin: marine or continental. This work shows for the first time the size distribution of aerosols registered at the Pierre Auger Observatory. The correlations found between mass and particle concentrations (total and for different size ranges) and HYSPLIT air mass trajectories, confirm that the latter can be employed as a useful tool to infer the sources, evolution and characteristics of the aerosols.

## 1 Introduction

Sites for astrophysical measurements, particularly those that observe weak light signals, need clean atmospheric conditions. Several projects of this type are either operating or being planned in the Andean region of Argentina. The study presented in this work was performed at the Pierre Auger Observatory of ultra-high-energy cosmic rays (`www.auger.org`), located close to the town of Malargüe [1]. The observatory has a hybrid design made of surface and fluorescence detectors (SD and FD, respectively). The FD system is composed of four stations that totalise 27 telescopes devoted to capture the fluorescence signals (in the 300–450 nm range) produced by the de-excitation of atmospheric nitrogen, previously excited by the charged particles of a cosmic ray shower induced by a primary cosmic ray entering into the atmosphere. A good knowledge of the atmospheric attenuation of the fluorescence light when it travels from the shower to the telescopes is necessary to make a reliable reconstruction of the primary cosmic ray properties. Atmospheric constituents attenuate this light, aerosols (particles suspended in the atmosphere) being of major importance in this process. Being highly variable in space and time, the aerosols have to be monitored continuously. Different devices are installed at the Pierre Auger Observatory to monitor the atmospheric variables, many of

[a] e-mail: `micheletti@ifir-conicet.gov.ar`

them devoted to measure the aerosol properties: the vertical aerosol depth (VAOD), the Angström coefficient and the aerosol phase function [2].

In 2008, to add more information about these atmospheric particles to that already provided by the instruments of the monitoring setup of the observatory, aerosol concentration measurements began to take place at the observatory, initially by collecting aerosols in filters and measuring the deposited mass by gravimetric analysis [3]. Very low aerosol concentrations were obtained during the Austral winter 2008, $7(1.1)\,\mu g/m^3$ [sd $= 4.5\,\mu g/m^3$] being the mean $PM_{10}$ concentration value at the FD station of Coihueco (35° 06′ 50.52″ S, 69° 35′ 59.33″ W, 1690 m ASL) at 6.3 m above ground level (AGL). $PM_{10}$ (particulate matter with $d \leq 10\,\mu m$) refers to the concentration of particles with aerodynamic diameter ($d$) up to $10\,\mu m$. Analogous definitions are made for other PM size ranges.

The aerosol concentrations given by this method were obtained from samples corresponding to a 24 hours deposition of aerosol mass on filters. However, the aerosol situation can significantly change throughout a day. In order to have a more detailed knowledge of the aerosol concentration evolution, a Grimm 1.109 aerosol spectrometer was installed at the same FD station. With this instrument, concentration values were registered every 5 minutes, at essentially surface level (about 1.7 m AGL). Counting with aerosol concentration data throughout the day gives the possibility to perform a correlation between these data and particle trajectories arriving at the monitored site, in order to infer the sources of the aerosols present there. In this work, a detailed analysis of air mass trajectories reaching the Pierre Auger Observatory, calculated with the HYSPLIT program [4,5], has been compared with Grimm 1.109 concentration data for the winter period of 2011. The winter period is chosen for this study because aerosol characterization and concentration determination from samples of particulate matter collected at the Auger Observatory, have previously been performed for a winter season [3]. In previous work, the air masses arriving at the observatory were compared with VAOD values measured by a Central Laser Facility (CLF), one of the devices of the aerosol monitoring system at the Pierre Auger Observatory [6–8]. However, CLF data are taken only during the nights of FD operation, while the Grimm 1.109 measurements provide a continuous data set for the whole day (diurnal and nocturnal hours) and for all the days (not only for FD data-taking periods). Another advantage of Grimm 1.109 is that it gives information about the size distribution of aerosols (obtained for the first time at the observatory). This is useful for being related with the analysis of sources and evolution of aerosols arriving at the observatory, performed by using the HYSPLIT trajectories. This work complements and extends the previous ones by finding a correlation between mass and particle concentration (total and as a function of size) near surface and air mass behaviour, giving an insight into the link between the origin and characteristics of the aerosols present at the Auger Observatory. It also sheds light on the sources and time-space evolution of the particles collected and analysed in the framework of the aerosol characterization studies performed at the observatory [3].

Knowledge of the aerosol characteristics is useful for models of fluorescence light propagation in the atmosphere used in cosmic ray shower reconstruction programs. The present study exceeds its local application and is based on the following method: to find a correlation between aerosol measurements and particle trajectories at a typical Andean Argentinean place, which can then be used to infer the aerosol characteristics at the same site or at other similar ones in the region by using air mass displacement models in situations for which local measurements are not available.

## 2 Measurements and analysis techniques

Data registered with a portable laser aerosol spectrometer and dust monitor (Grimm 1.109), installed at the FD building of Coihueco, at about 1.7 m AGL, to perform local superficial aerosol concentration measurements, are analysed in this work for the June–September 2011 period. This entire period of four months of cold temperatures can be considered as the extended southern winter. The Grimm 1.109 registered data on mass concentration ($\mu g/m^3$), every 5 minutes, for aerosol size channels from 0.22 to $32\,\mu m$. The principle of operation is based on an internal laser (655 nm) and a model for the light dispersion produced by the aerosols contained in the flux of air driven into the apparatus by a pump (flow rate 1.2 L/min). HYSPLIT is an air-modelling program, developed by NOAA (National Oceanic and Atmospheric Administration, USA), used in calculations of air mass displacements between different sites. It is useful to determine the sources and evolution of aerosols. HYSPLIT provides backward/forward trajectories from a place, chosen by selecting its coordinates and altitude, by moving to the past/to the future in time from an initial selected date and time. In this way, HYSPLIT links different regions by their aerosols and air mass transport. More details about this program and its use for identifying air masses arriving at the Pierre Auger Observatory can be found elsewhere [7,8]. In the present work, one backward trajectory per hour, computed over 48 hours, was evaluated at the arrival site of the Pierre Auger Observatory (35° S, 69° W, 1400 m ASL) at 500 m height above it. The trajectories were performed for the period of concentration measurements with the Grimm 1.109 aerosol spectrometer: June, July (from 14 July to the end of month), August and September. Meteorological data (wind vector, ambient temperature, surface pressure and height) from the GDAS (Global Data Assimilation System, NOAA) model [9], for the site of the Pierre Auger Observatory, were used to produce the HYSPLIT trajectories. The validity of the use of the GDAS data for local weather data at the Auger Observatory was established by the Auger Collaboration, based on their good agreement with ground-based weather stations and meteorological radiosonde launches [10].

## 3 Results

### 3.1 Local aerosol concentrations and air mass trajectories correlation

Total mass concentration data $PM_{tot}$ (corresponding to all the aerosols of diameters bigger than 0.22 $\mu$m) provided by the Grimm 1.109 aerosol spectrometer every 5 minutes, are presented in fig. 1(a) for the four months of the 2011 Austral winter. Concentrations are higher for June and September and lower for July and August. Table 1 presents the data on mass and particle concentration at different size intervals. Figure 1(b) shows the mean mass concentration, given by Grimm 1.109, for each month, for each size channel, normalised by the width of the size range (mean mass size distribution). The area under each histogram is the mean value of the total concentration ($PM_{tot}$) for each month. Figure 2 shows the normalised mean particle concentration (mean particle size distribution) for the four months.

It is evident from figs. 1 and 2 and table 1 that August 2011, the month with the cleanest atmosphere, as given by the lowest mean mass concentration $PM_{tot}$ value, is also the month that shows a different behaviour in the size range distribution of the concentration values. In fact, it differs significantly from the other months due to its higher percentage of the smaller particles relative to the larger ones. $PM_{0.5}$, the mean concentration of particles of diameter smaller than 0.5 $\mu$m, represents around 20% of $PM_{tot}$ in August but does not surpass a mean value of 7.8% during the other months for mass concentration. When considering particle concentration, this size range contributes 98% in August, this contribution being lower for the other months. Besides, the contribution of $PM_{2.5}$ in $PM_{10}$ (where $PM_{2.5} + PM_{2.5\text{-}10} = PM_{10}$) and in $PM_{tot}$ is considerably higher in August than in the rest of the period. Considering the mean mass concentration per size intervals of 1 $\mu$m width, in the range 1–10 $\mu$m (the area under the curve for each interval of 1 $\mu$m in the mentioned range, as shown in fig. 1(b) and stated in table 1), one obtains a peak in concentration in the 4–5 $\mu$m size interval (being denoted as $PM_{4\text{-}5}$), of around 20% for the different months, except for August where a comparable value occurs for $PM_1$ ($d \leq 1\,\mu$m) where the peak of concentration takes place. The dominant concentration values per size interval for August are evidently shifted towards lighter aerosols, meaning an appreciable over-abundance of them in the total content of particles. This is in comparison with the other months and also with the mean of the whole analysed period. This can be clearly noticed in fig. 2 for the mean particle size distribution (mean particle concentration distribution, normalized by the size range width). In fact, the August particle concentration is the lowest one for particles bigger than about 1 $\mu$m but it is higher than July for particles smaller than this size. It surpasses June at the lowest size ranges, (up to 0.3 $\mu$m) even when the mean mass concentration $PM_{tot}$ is considerably lower for August than June. This fact shows the overabundance of small particles with respect to the bigger ones in August 2011.

Every hour, the concentration value obtained by Grimm 1.109 was correlated with a HYSPLIT backward trajectory, initiated at the Pierre Auger Observatory, at 500 m AGL, in order to investigate the connection between the aerosols present at the observatory and the behaviour of the air masses reaching it. This method permits one to infer the sources and evolution of the aerosols found in the site of interest. The validity of this approach is based on the fact that we are linking the surface Grimm data with HYSPLT air mass trajectories arriving at an altitude included in the planetary boundary layer (PBL), where the aerosols are considered to be well enough mixed to be homogenised inside it. An analysis of Raman lidar data at the Pierre Auger Observatory has showed that all the monthly mean values for the height of the PBL were bigger than the 500 m AGL considered in this analysis. The mean value found for the "winter" half year (April to September) average of the height of the PBL was 1049[664] m [11].

Figure 3 shows two-dimensional diagrams, longitude *versus* latitude, in which all regions traversed by an air mass path during the 48 h period previous to its arrival to the Pierre Auger Observatory, were depicted. The diagrams correspond to the four months of the winter period. The black star represents the Pierre Auger Observatory. The black line represents the South American coast. Colours indicate the frequency of a traversed region, from red (more frequent) to blue (less frequent). By observing the diagrams it can be noted that August presents lower density of trajectories over the continent than the other months (represented by the lower presence of green colour over the continental areas). In order to quantify this observation, we defined a parameter of continentality in the following way: $C = 100 \times t_{land}/(t_{sea} + t_{land})$. This parameter, calculated for each trajectory, provides the percentage of time in which it traverses land areas with respect to its total travelling time of 48 h (which consists of the addition of its time over the sea and its time over the land). If a 48 h trajectory is completely over the land, $C$ is 100%. This parameter was calculated for every trajectory and a mean value $\langle C \rangle$ of it was obtained for four different data sets, one for each month of winter. The result is the following: $\langle C_{Jun} \rangle = 78\%$ (sd = 28%), $\langle C_{Jul} \rangle = 77\%$ (sd = 28%), $\langle C_{Aug} \rangle = 72\%$ (sd = 27%) and $\langle C_{Sep} \rangle = 77\%$ (sd = 29%). The mean continentality ($\langle C \rangle$) is almost the same for the different months of winter, except for August in which it is lower (6.5% lower than in July and September and 7.7% lower than in June). This higher proportion of time travelling over the sea in comparison with the time travelling over the land for the trajectories for August can be the reason for the lower concentrations found for this month, as well as its higher proportion of small particles with respect to large ones. This is in agreement with the results found by the analysis of aerosols collected on filters at the observatory: most of them are aluminosilicates that come from the soil of the Andean region [3].

**Table 1.** Mean mass and particle concentration values for different aerosol size ranges and percent contribution of each range to the total concentration $PM_{tot}$ for June, July, August and September 2011, and for the whole period, obtained from Grimm 1.109 measurements performed at Coihueco FD building of the Auger Observatory. (*): Values that are almost 100% of the total concentration and that can be considered 100% when the error band is taken into account.

| June year 2011 | | | | |
|---|---|---|---|---|
| Fraction | Mass concentration (std. err.) [$\mu g/m^3$] | % | Particle concentration (std. err.) [particle/$m^3$] | % |
| $PM_{tot}$ | 16.81 (0.46) | 100 | 3.98E7 (7.3E5) | 100 |
| $PM_{0.5}$ | 0.77 (0.02) | 4.58 | 3.80E7 (7.1E5) | 95.48 |
| $PM_{2.5}$ | 2.58 (0.04) | 15.35 | 3.96E7 (7.2E5) | 99.50 |
| $PM_{2.5\text{-}10}$ | 13.43 (0.42) | 79.89 | 2.12E5 (4.9E3) | 0.53 |
| $PM_{10}$ | 16.01 (0.45) | 95.24 | 3.98E7 (*) (7.3E5) | 100 |
| $PM_{>10}$ | 0.79 (0.03) | 4.70 | 4.9E2 (1.5E1) | 1E-3 |
| $PM_{0.5\text{-}1.0}$ | 0.34 (0.01) | 2.02 | 1.23E6 (2.1E4) | 3.09 |
| $PM_{1}$ | 1.11 (0.02) | 6.60 | 3.92E7 (7.2E5) | 98.49 |
| $PM_{1\text{-}2}$ | 0.71 (0.01) | 4.22 | 2.60E5 (4.4E3) | 0.65 |
| $PM_{2\text{-}3}$ | 1.99 (0.04) | 11.84 | 1.43E5 (2.6E3) | 0.36 |
| $PM_{3\text{-}4}$ | 2.77 (0.06) | 16.48 | 7.5E4 (1.5E3) | 0.19 |
| $PM_{4\text{-}5}$ | 3.43 (0.10) | 20.40 | 4.3E4 (1.3E3) | 0.11 |
| $PM_{5\text{-}6}$ | 2.15 (0.09) | 12.79 | 1.28E4 (5.6E2) | 0.03 |
| $PM_{6\text{-}7}$ | 1.69 (0.08) | 10.05 | 8.5E3 (3.9E2) | 0.02 |
| $PM_{7\text{-}8}$ | 1.03 (0.05) | 6.13 | 3.0E3 (1.5E2) | 0.01 |
| $PM_{8\text{-}9}$ | 0.66 (0.03) | 3.93 | 1.27E3 (5.3E1) | 3E-3 |
| $PM_{9\text{-}10}$ | 0.47 (0.02) | 2.80 | 6.8E2 (2.2E1) | 2E-3 |
| July year 2011 | | | | |
| Fraction | Mass concentration (std. err.) [$\mu g/m^3$] | % | Particle concentration (std. err.) [particle/$m^3$] | % |
| $PM_{tot}$ | 6.30 (0.31) | 100 | 2.55E7 (7.1E5) | 100 |
| $PM_{0.5}$ | 0.49 (0.01) | 7.78 | 2.48E7 (6.9E5) | 97.25 |
| $PM_{2.5}$ | 1.17 (0.03) | 18.57 | 2.54E7 (7.1E5) | 99.61 |
| $PM_{2.5\text{-}10}$ | 4.45 (0.23) | 70.63 | 7.4E4 (4.1E3) | 0.29 |
| $PM_{10}$ | 5.62 (0.25) | 89.20 | 2.55E7 (*) (7.1E5) | 100 |
| $PM_{>10}$ | 0.68 (0.17) | 10.79 | 1.8E2 (0.6E1) | 7E-4 |
| $PM_{0.5\text{-}1.0}$ | 0.13 (0.003) | 2.06 | 5.1E5 (1.5E4) | 2.00 |
| $PM_{1}$ | 0.62 (0.02) | 10.39 | 2.53E7 (7.1E5) | 99.22 |
| $PM_{1\text{-}2}$ | 0.24 (0.008) | 3.81 | 8.7E4 (2.6E3) | 0.34 |
| $PM_{2\text{-}3}$ | 0.78 (0.04) | 13.07 | 5.7E4 (2.6E3) | 0.22 |
| $PM_{3\text{-}4}$ | 0.94 (0.06) | 15.75 | 2.5E4 (1.7E3) | 0.10 |
| $PM_{4\text{-}5}$ | 1.26 (0.08) | 20.00 | 1.6E4 (1.0E3) | 0.06 |
| $PM_{5\text{-}6}$ | 0.67 (0.04) | 10.63 | 4.0E3 (2.5E2) | 0.02 |
| $PM_{6\text{-}7}$ | 0.51 (0.03) | 8.10 | 2.6E3 (1.6E2) | 0.01 |
| $PM_{7\text{-}8}$ | 0.29 (0.02) | 4.60 | 8.3E2 (5.8E1) | 3E-3 |
| $PM_{8\text{-}9}$ | 0.19 (0.008) | 3.02 | 3.6E2 (1.7E1) | 1E-3 |
| $PM_{9\text{-}10}$ | 0.14 (0.004) | 2.22 | 2.0E2 (0.6E1) | 8E-4 |

**Table 1.** Continued.

| August year 2011 | | | | |
|---|---|---|---|---|
| Fraction | Mass concentration (std. err.) [$\mu$g/m$^3$] | % | Particle concentration (std. err.) [particle/m$^3$] | % |
| $PM_{tot}$ | 3.75 (0.07) | 100 | 4.04E7 (8.0E5) | 100 |
| $PM_{0.5}$ | 0.75 (0.01) | 20 | 3.96E7 (8.0E5) | 98.02 |
| $PM_{2.5}$ | 1.38 (0.02) | 36.8 | 4.04E7 (*) (8.0E5) | 100 |
| $PM_{2.5\text{-}10}$ | 2.16 (0.04) | 57.6 | 4.13E4 (8.3E2) | 0.10 |
| $PM_{10}$ | 3.54 (0.06) | 94.4 | 4.04E7 (*) (8.0E5) | 100 |
| $PM_{>10}$ | 0.21 (0.01) | 5.6 | 1.0E2 (0.3E1) | 3E-4 |
| $PM_{0.5\text{-}1.0}$ | 0.15 (0.003) | 4.27 | 6.3E5 (1.0E4) | 1.56 |
| $PM_1$ | 0.91 (0.02) | 24.27 | 4.02E7 (8.0E5) | 99.50 |
| $PM_{1\text{-}2}$ | 0.24 (0.005) | 6.4 | 9.1E4 (1.8E3) | 0.23 |
| $PM_{2\text{-}3}$ | 0.56 (0.01) | 14.93 | 4.18E4 (7.1E2) | 0.10 |
| $PM_{3\text{-}4}$ | 0.50 (0.01) | 13.33 | 1.36E4 (3.2E2) | 0.03 |
| $PM_{4\text{-}5}$ | 0.53 (0.01) | 14.13 | 6.6E3 (1.4E2) | 0.02 |
| $PM_{5\text{-}6}$ | 0.29 (0.006) | 7.73 | 1.71E3 (3.5E1) | 4E-3 |
| $PM_{6\text{-}7}$ | 0.22 (0.005) | 5.87 | 1.12E3 (2.3E1) | 3E-3 |
| $PM_{7\text{-}8}$ | 0.13 (0.003) | 3.47 | 3.8E2 (1.2E1) | 9E-4 |
| $PM_{8\text{-}9}$ | 0.09 (0.002) | 2.40 | 1.75E2 (0.4E1) | 4E-4 |
| $PM_{9\text{-}10}$ | 0.07 (0.002) | 1.87 | 1.06E2 (0.3E1) | 3E-4 |
| September year 2011 | | | | |
| Fraction | Mass concentration (std. err.) [$\mu$g/m$^3$] | % | Particle concentration (std. err.) [particle/m$^3$] | % |
| $PM_{tot}$ | 18.61 (0.28) | 100 | 5.63E7 (6.7E5) | 100 |
| $PM_{0.5}$ | 1.03 (0.01) | 5.53 | 5.43E7 (6.6E5) | 96.45 |
| $PM_{2.5}$ | 3.16 (0.04) | 16.98 | 5.61E7 (6.7E5) | 99.64 |
| $PM_{2.5\text{-}10}$ | 13.88 (0.22) | 74.58 | 2.23E5 (3.6E3) | 0.40 |
| $PM_{10}$ | 17.04 (0.26) | 91.56 | 5.63E7 (*) (6.7E5) | 100 |
| $PM_{>10}$ | 1.58 (0.03) | 8.49 | 9.1E2 (1.6E1) | 2E-3 |
| $PM_{0.5\text{-}1.0}$ | 0.39 (0.007) | 2.10 | 1.39E6 (2.4E4) | 2.47 |
| $PM_1$ | 1.42 (0.01) | 7.63 | 5.56E7 (6.7E5) | 98.76 |
| $PM_{1\text{-}2}$ | 0.86 (0.02) | 4.62 | 3.19E5 (5.8E3) | 0.57 |
| $PM_{2\text{-}3}$ | 2.25 (0.04) | 12.09 | 1.63E5 (2.6E3) | 0.29 |
| $PM_{3\text{-}4}$ | 2.92 (0.05) | 15.69 | 7.9E4 (1.3E3) | 0.14 |
| $PM_{4\text{-}5}$ | 3.40 (0.05) | 18.27 | 4.25E4 (6.7E2) | 0.08 |
| $PM_{5\text{-}6}$ | 2.05 (0.03) | 11.02 | 1.22E4 (1.9E2) | 0.02 |
| $PM_{6\text{-}7}$ | 1.64 (0.03) | 8.81 | 8.2E3 (1.3E2) | 0.01 |
| $PM_{7\text{-}8}$ | 1.08 (0.02) | 5.80 | 3.08E3 (4.9E1) | 5-E-3 |
| $PM_{8\text{-}9}$ | 0.78 (0.01) | 4.19 | 1.47E3 (2.4E1) | 3E-3 |
| $PM_{9\text{-}10}$ | 0.63 (0.01) | 3.39 | 9.1E2 (1.6E1) | 2E-3 |

**Table 1.** Continued.

| June–September year 2011 | | | | |
|---|---|---|---|---|
| Fraction | Mass concentration (std. err.) [$\mu$g/m$^3$] | % | Particle concentration (std. err.) [particle/m$^3$] | % |
| $PM_{tot}$ | 11.68 (0.16) | 100 | 4.21E7 (3.8E5) | 100 |
| $PM_{0.5}$ | 0.79 (0.01) | 6.76 | 4.07E7 (3.7E5) | 96.67 |
| $PM_{2.5}$ | 2.15 (0.02) | 18.41 | 4.19E7 (3.8E5) | 99.52 |
| $PM_{2.5\text{-}10}$ | 8.71 (0.13) | 74.57 | 1.41E5 (1.8E3) | 0.33 |
| $PM_{10}$ | 10.86 (0.15) | 92.98 | 4.21E7 ($^*$) (3.8E5) | 100 |
| $PM_{>10}$ | 0.82 (0.03) | 7.02 | 4.4E2 (0.6E1) | 1E-3 |
| $PM_{0.5\text{-}1.0}$ | 0.26 (0.003) | 2.23 | 9.72E5 (9.7E3) | 2.31 |
| $PM_1$ | 1.05 (0.01) | 8.99 | 4.17E7 (3.8E5) | 99.05 |
| $PM_{1\text{-}2}$ | 0.53 (0.01) | 4.54 | 1.97E5 (2.2E3) | 0.47 |
| $PM_{2\text{-}3}$ | 1.44 (0.02) | 12.33 | 1.04E5 (1.E3) | 0.25 |
| $PM_{3\text{-}4}$ | 1.83 (0.02) | 15.67 | 4.98E4 (6.5E2) | 0.12 |
| $PM_{4\text{-}5}$ | 2.20 (0.03) | 18.84 | 2.74E4 (4.3E2) | 0.07 |
| $PM_{5\text{-}6}$ | 1.32 (0.03) | 11.30 | 7.9E3 (1.6E2) | 0.02 |
| $PM_{6\text{-}7}$ | 1.04 (0.02) | 8.90 | 5.2E3 (1.1E2) | 0.01 |
| $PM_{7\text{-}8}$ | 0.65 (0.01) | 5.57 | 1.87E3 (4.3E1) | 4E-3 |
| $PM_{8\text{-}9}$ | 0.44 (0.01) | 3.77 | 8.5E2 (1.6E1) | 2E-3 |
| $PM_{9\text{-}10}$ | 0.35 (0.01) | 3.00 | 5.0E2 (0.8E1) | 1E-3 |

A shorter travel of air masses over the continental areas (mainly belonging to Andean zones, see fig. 3) would cause a lower content of aerosols, especially the bigger ones that consist typically of dust of the Andean desert-like region. Previous analysis of air mass trajectories and VAOD data from the CLF, as mentioned in sect. 1, performed throughout a year, linked clear atmospheric conditions with air masses coming from the Pacific Ocean [7].

The results provided by the Grimm 1.109 confirm the previous ones and add information about the size distribution effect due to the origin and evolution of the air masses. In order to further clarify the correspondence between the clean and hazy atmospheric conditions and the behaviour of air masses, an analysis of their arrival directions when reaching the Pierre Auger Observatory was performed. To do this, each 48 h air mass trajectory was subdivided into two 24 h sub-trajectories and the most recent one (that corresponds to distances closer to the observatory) was chosen for the analysis. The shorter period (the 24 h sub-trajectory) prevents abrupt changes in air mass path direction that may happen in a longer period. The air mass trajectories taken into account for this approach were the ones that arrived at the observatory at a time in which the Grimm 1.109 concentration data were below (clean atmosphere) or above (hazy atmosphere) fixed boundary concentration levels. The study was performed for $PM_{10}$, $PM_{2.5}$ and $PM_{2.5\text{-}10}$ (where the latter ones represent the fine and coarse fractions of $PM_{10}$). Taking into account that the $PM_{2.5}$ and $PM_{2.5\text{-}10}$ fractions consist of approximately 20% and 80% of $PM_{10}$, respectively, as can be seen from table 1, for the whole June-to-September period (behaviour that occurs also for the individual months, except for August that shows an over-abundance of particles of the fine fraction), the boundaries for the clear and hazy atmospheric conditions were chosen in accordance with these proportions.

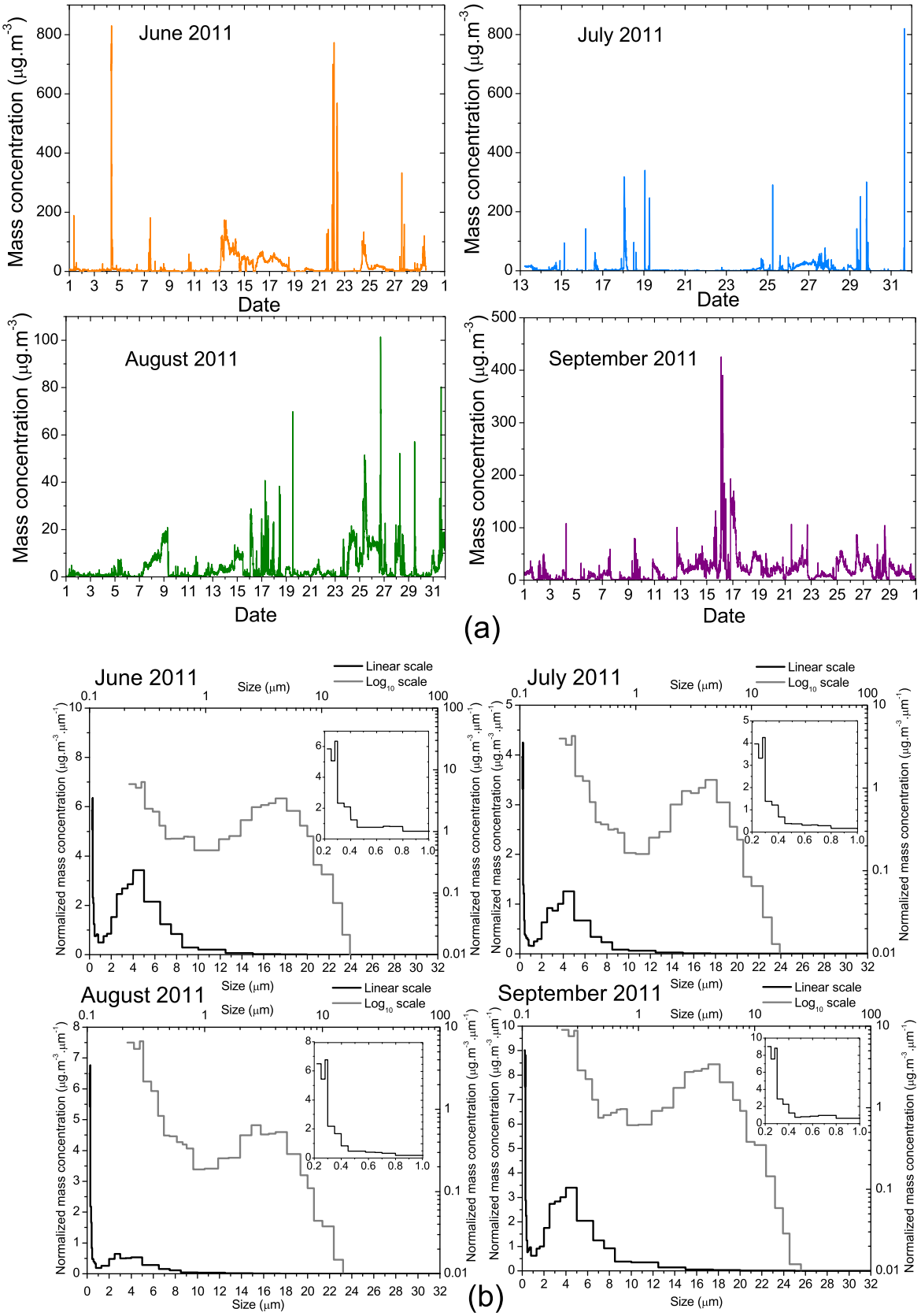


**Fig. 1.** (a) Total mass concentration given by Grimm 1.109, every 5 minutes, for the four winter months of 2011. (b) Mean mass concentration for each month of winter 2011, for different size intervals, normalised by the width of the interval (mean mass size distribution), obtained from the Grimm 1.109 data. Linear scale: black line, bottom $x$-axis, left $y$-axis. Log scale: gray line, top $x$-axis, right $y$-axis. Inside each graphic the lowest diameter range is expanded (in linear scale).

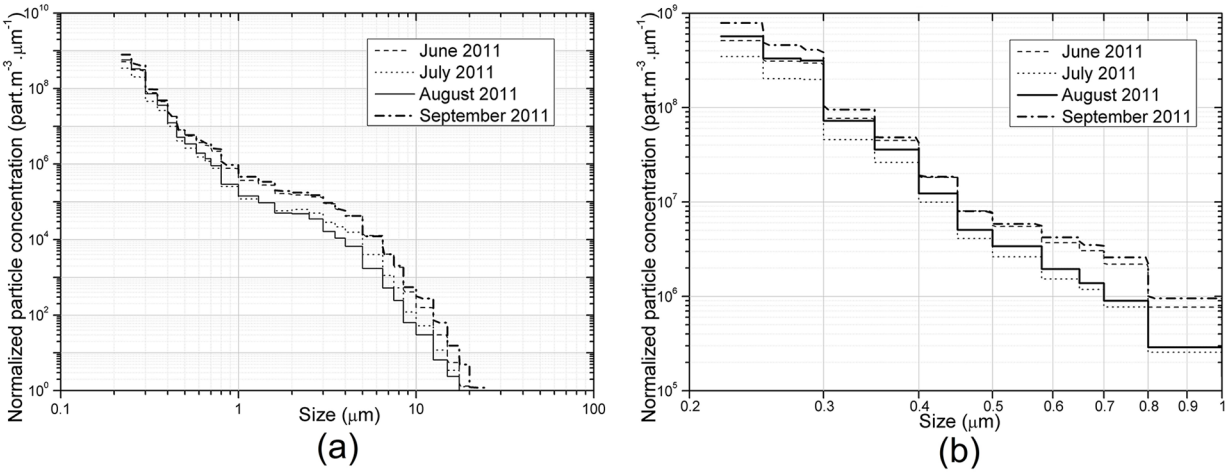


**Fig. 2.** (a) Mean particle concentration for the four months of winter 2011, normalized by the width of the interval (mean particle size distribution), obtained from the Grimm 1.109 data. (b) The size range up to 1 $\mu$m is expanded.

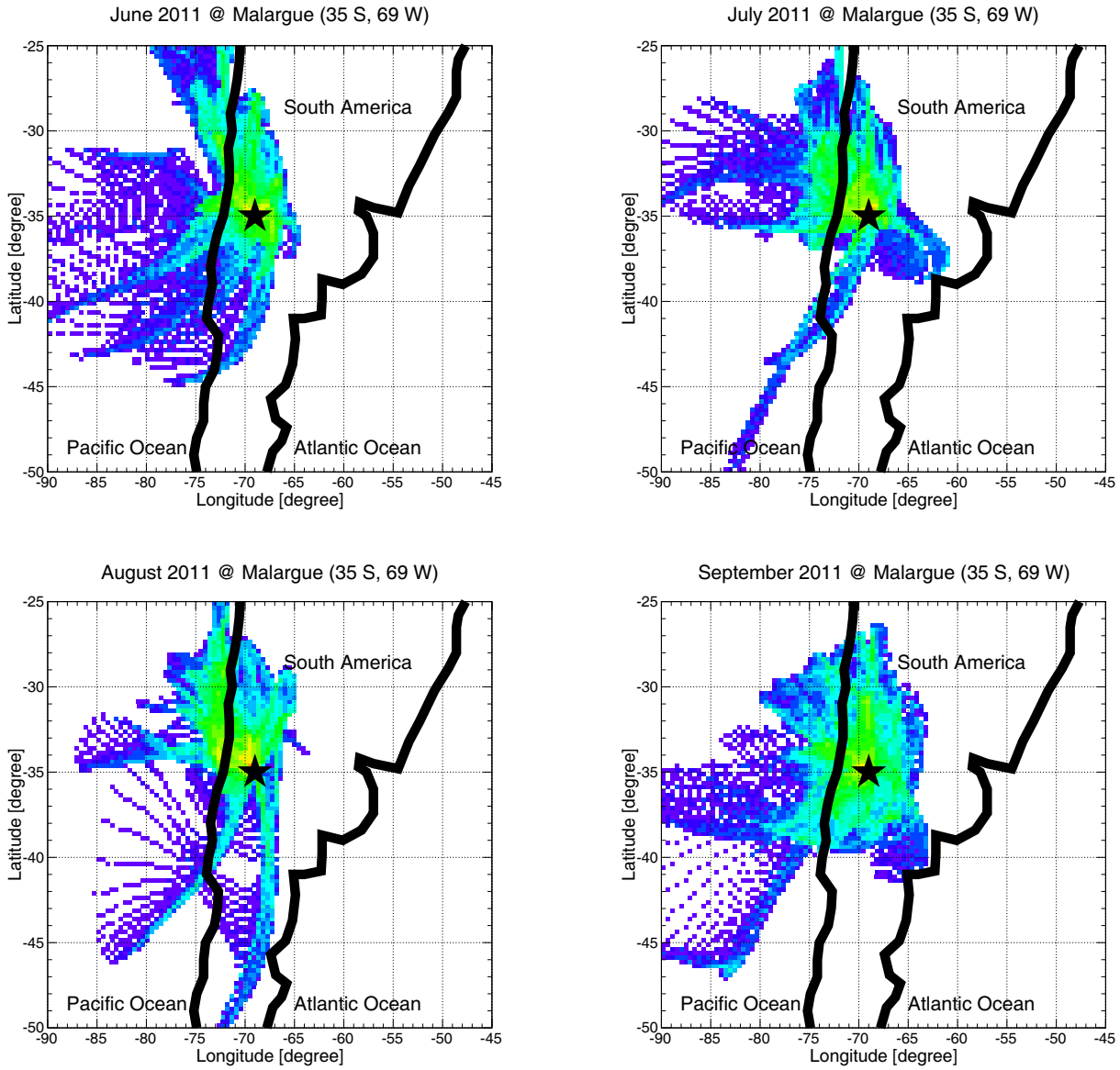


**Fig. 3.** Distribution of 48 h HYSPLIT backward trajectories (one per hour, at a start altitude fixed at 500 m AGL) from the site of the Pierre Auger Observatory, by month of winter 2011. The black star represents the observatory and the black line the South American coast. Colours indicate the frequency of a region, from red (more frequent) to blue (less frequent). (When printed in gray scale: from light gray (more frequent) to dark gray (less frequent)).

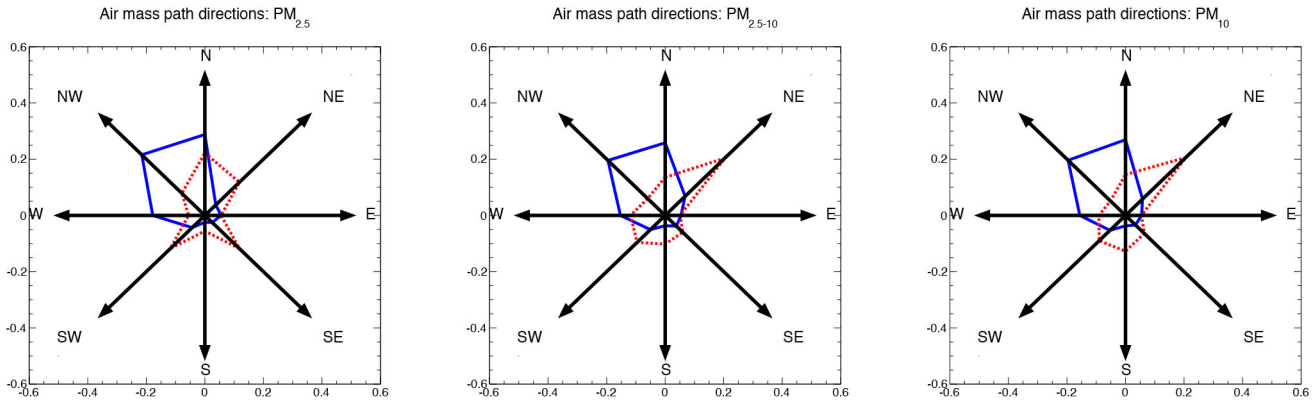


**Fig. 4.** Polar histograms showing the probability density function of the arrival directions of the HYSPLIT air masses reaching the Pierre Auger Observatory for two selected situations, clean (blue continuous line) and hazy (red dotted line) (as given by Grimm 1.109 measurements), and for three particle size ranges: $PM_{2.5}$ (left), $PM_{2.5\text{-}10}$ (centre) and $PM_{10}$ (right). Period: June–September 2011.

These boundaries are defined as follows: $PM_{2.5} \leq 0.5\,\mu g/m^3$, $PM_{2.5\text{-}10} \leq 2.0\,\mu g/m^3$ and $PM_{10} \leq 2.5\,\mu g/m^3$ for clear conditions, and $PM_{2.5} \geq 12.5\,\mu g/m^3$, $PM_{2.5\text{-}10} \geq 50.0\,\mu g/m^3$ and $PM_{10} \geq 62.5\,\mu g/m^3$ for hazy conditions. Figure 4 consists of three polar histograms showing the arrival directions of the HYSPLIT air masses reaching the Pierre Auger Observatory for two selected situations, clean and hazy, and for three particle size ranges, $PM_{2.5}$, $PM_{2.5\text{-}10}$ and $PM_{10}$.

It corresponds to the period June–September 2011. Each histogram has 8 bins consisting of the arrival directions defined as: North/N ($0° \pm 22.5°$), North-East/NE ($45° \pm 22.5°$), East/E ($90° \pm 22.5°$), South-East/SE ($135° \pm 22.5°$), South/S ($180° \pm 22.5°$), South-West/SW ($225° \pm 22.5°$), West/W ($270° \pm 22.5°$), North-West/NW ($315° \pm 22.5°$). For each analysed PM range, the backward trajectories were divided into two groups: clean and hazy cases, represented by the blue and red colours in the figures, respectively, according to the boundaries in concentration values specified above. For each air mass sub-trajectory of a given group (clean or hazy), corresponding to the period of time of the last 24 h before its arrival to the site, its direction is obtained as the most probable value of the sub-directions of the 24 h sub-path (one per hour). The different directions recorded are then plotted in the polar histogram, in which the angular coordinate represents the arrival direction as defined above and the radial coordinate represents the probability density for a trajectory to be in a particular bin of direction. For each selected group (clean or hazy), this probability density is obtained as the addition of all the trajectories with a given direction divided by the total number of trajectories of this group. So, this graphic represents the probability density function, *i.e.* the distribution of the origins, normalised to the number of trajectories. Also, the continentality values ($C$) were calculated for each trajectory of this analysis and the mean values for each group and each PM size range were obtained: $\langle C_{2.5}\rangle = 64\%$ (sd = 30%), $\langle C_{2.5\text{-}10}\rangle = 68\%$ (sd = 30%) and $\langle C_{10}\rangle = 68\%$ (sd = 30%) for clear conditions, and $\langle C_{2.5}\rangle = 72\%$ (sd = 26%), $\langle C_{2.5\text{-}10}\rangle = 77\%$ (sd = 24%) and $\langle C_{10}\rangle = 77\%$ (sd = 23%) for hazy conditions. Figure 4 shows an evident dominance of mass trajectories arriving at the observatory from the NW direction during clear atmospheric situations for all the PM ranges analysed. However, the privileged directions differs for the different PM considered during the hazy case. For $PM_{2.5\text{-}10}$ and $PM_{10}$, air masses mostly arrive from the NE, for the fine fraction $PM_{2.5}$ this tendency is very weak, resulting in an almost symmetric graphic along the S–N axis. We can conclude that, in general, clear atmospheric conditions are linked to winds coming from the ocean and that hazy conditions are linked to winds coming from the continental areas, mainly from the NE. This is in agreement with the higher mean continentality values ($\langle C\rangle$) found for the hazy conditions than for the clear ones. The atypical behaviour of the air mass arrival directions for the hazy situation for $PM_{2.5}$ can be understood by the fact that sea aerosols, which are maintained by mechanical lifting by the wind, are mostly included in this particle size range (as was found by experiments performed in remote areas of the central Pacific Ocean [12]).

So, hazy conditions for fine particles can be caused either by marine aerosols from the Pacific Ocean (NW direction) or from anthropogenic aerosols coming principally from the north or NE (it is important to note that most important urban sites that could influence the atmospheric conditions of the observatory are placed north to it while south to it is the Patagonia region, one of the less populated areas of the world).

Figure 5 and table 2 present information about the cities (marked with the large filled circles) that are in the area affected by the air masses shown in fig. 3. Even if Chilean cities placed in the mentioned area are also included, it is important to recognise that the Andean mountains consists of an important natural barrier for local Chilean pollution generated in big cities which remains mostly confined in them [13]. The winds predominantly arrive from the West direction to Argentina, East of the Andes, after crossing the mountains. This phenomenon converts this region into one with a specially clean atmosphere and remarkable good conditions for doing astrophysics science [14]. Figure 6 shows the topographic profiles centered in the measurement site of Coihueco.


**Fig. 5.** Map showing the cities (marked with the large filled circles) in the area covered by HYSPLIT air mass trajectories in fig. 3. The FD site of Coihueco is marked with a star.

**Table 2.** Most important localities placed in the area affected by the air masses trajectories shown in fig. 3, listed by increasing latitude. Santa Rosa is only peripheral in fig. 3 (only involved in the July and September maps of air mass trajectories). The density of population is considerably higher at the North of Malargüe than at the South of it (Patagonia). Distance (in km) is considered along the straight line between Coihueco FD building and the corresponding locality. The pollution of Chilean cities (shaded in grey) remains mostly confined in the Western side of the Andes, not having a considerable effect in the Argentinean side (where the Pierre Auger Observatory is placed).

| Locality (and surrounding area) | Distance (km) | Coordinates (Lat. Long.) | Population |
|---|---|---|---|
| San Juan | 409.84 | 31°32′15″ S 68°32′11″ W | 480,000 |
| Mendoza | 256.25 | 32°53′00″ S 68°50′00″ W | 950,000 |
| Valparaíso (Chile) | 296.35 | 33°03′47″ S 71°38′22″ W | 980,000 |
| San Luis | 359.82 | 33°16′38″ S 66°21′09″ W | 170,000 |
| Santiago (Chile) | 214.52 | 33°26′16″ S 70°39′01″ W | 7,310,000 |
| San Rafael | 126.64 | 34°37′03″ S 68°20′08″ W | 190,000 |
| Talca (Chile) | 189.18 | 35°26′00″ S 71°40′00″ W | 250,000 |
| Malargüe | 40.89 | 35°28′28″ S 69°35′07″ W | 30,000 |
| Santa Rosa | 506.70 | 36°37′13″ S 64°17′26″ W | 120,000 |
| Concepción (Chile) | 364.09 | 36°50′00″ S 73°03′00″ W | 220,000 |
| Neuquén | 448.67 | 38°57′26″ S 68°02′44″ W | 230,000 |

A smaller mean continentality value ($\langle C \rangle$) found for the hazy case for $PM_{2.5}$, in comparison with the same case for $PM_{2.5\text{-}10}$ and $PM_{10}$, also suggests that atmospheres with an important content of fine aerosols can be caused by winds coming from the ocean. This could be the cause of NaCl crystals found in samples collected at Coihueco in winter, but salt flats in the region could also be responsible for them [3]. On the other hand, a high content of coarse aerosols, which presents bigger continentality values ($C$), can be related to an Andean desert soil origin. Direct particle sampling and analysis previously performed at the observatory support this conclusion [3].

The suspended dust is also driven by winds and its associated sizes are mainly in the $PM_{2.5\text{-}10}$ range [12]. It can be noted from fig. 4 and from the continentality values, that $PM_{10}$ follows the behaviour of its coarse fraction $PM_{2.5\text{-}10}$ as it represents approximately 80% of $PM_{10}$.

The monthly mean values of temperature provided by the Argentinean National Meteorological Service, registered during 2011 at the Aerodrome of Malargüe (35°30′ S, 69°35′ W, 1426 m ASL) between 6 a.m. and 9 p.m., are $\langle T_{\text{Jun}} \rangle = 5.5\,^{\circ}\text{C}$ (sd $= 5.7\,^{\circ}\text{C}$), $\langle T_{\text{Jul}} \rangle = 4.1\,^{\circ}\text{C}$ (sd $= 7.4\,^{\circ}\text{C}$), $\langle T_{\text{Aug}} \rangle = 5.6\,^{\circ}\text{C}$ (sd $= 6.0\,^{\circ}\text{C}$) and $\langle T_{\text{Sep}} \rangle = 12.5\,^{\circ}\text{C}$ (sd $= 6.9\,^{\circ}\text{C}$). Even if a correlation was found between cold weather and low aerosol content, especially when snow keeps the soil particles blocked under it [3], the monthly mean temperature values and the air mass study previously discussed,

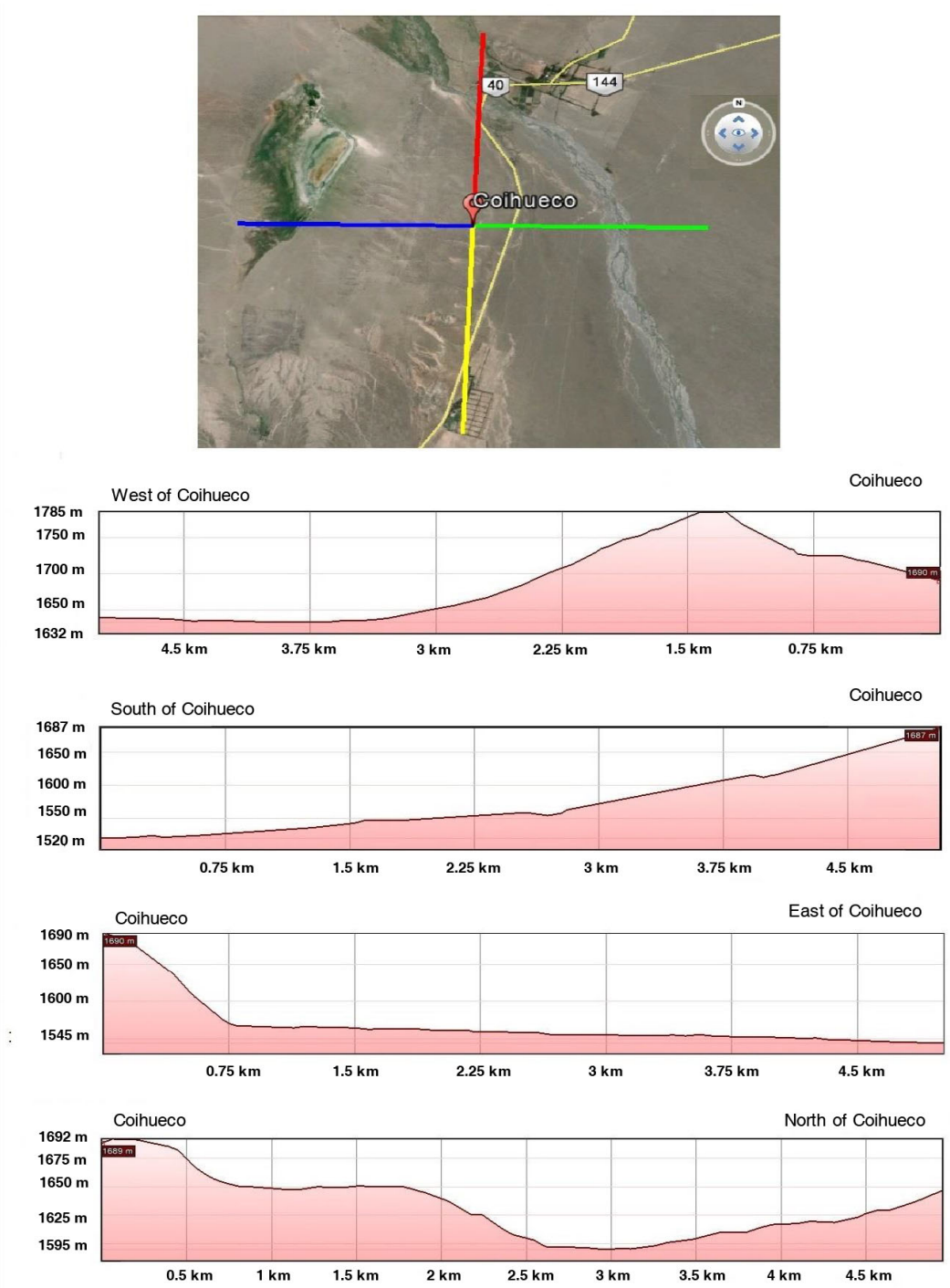


**Fig. 6.** Topographic profiles centered in the measurement site of Coihueco: (a) General satellite view of the site of Coihueco, centered in the cross that points in the four cardinal directions (the length of each arm of the cross is 5 km). (b), (c), (d), (e) altitudinal profiles in the four cardinal directions of 5 km of length shown in (a). Imagery: © 2017 CNES/Astrium, CNES/Spot Image, DigitalGlobe, Landsat/Copemicus. © 2017 Google.

suggest that air mass trajectories and the corresponding arrival directions at the Pierre Auger Observatory are the dominant causes in determining the aerosol mass concentration and the size distribution pattern at the observatory. This is especially observed for August, which is not the coldest month but the one with the lowest mean continentality value ($\langle C \rangle$) and which turns to be the one with the lowest mean mass concentration $PM_{tot}$ and with a particular aerosol size distribution pattern shifted towards smaller particles. This is in accordance with a more important proportion of sea aerosols (of smaller sizes) carried by winds towards the site of study.

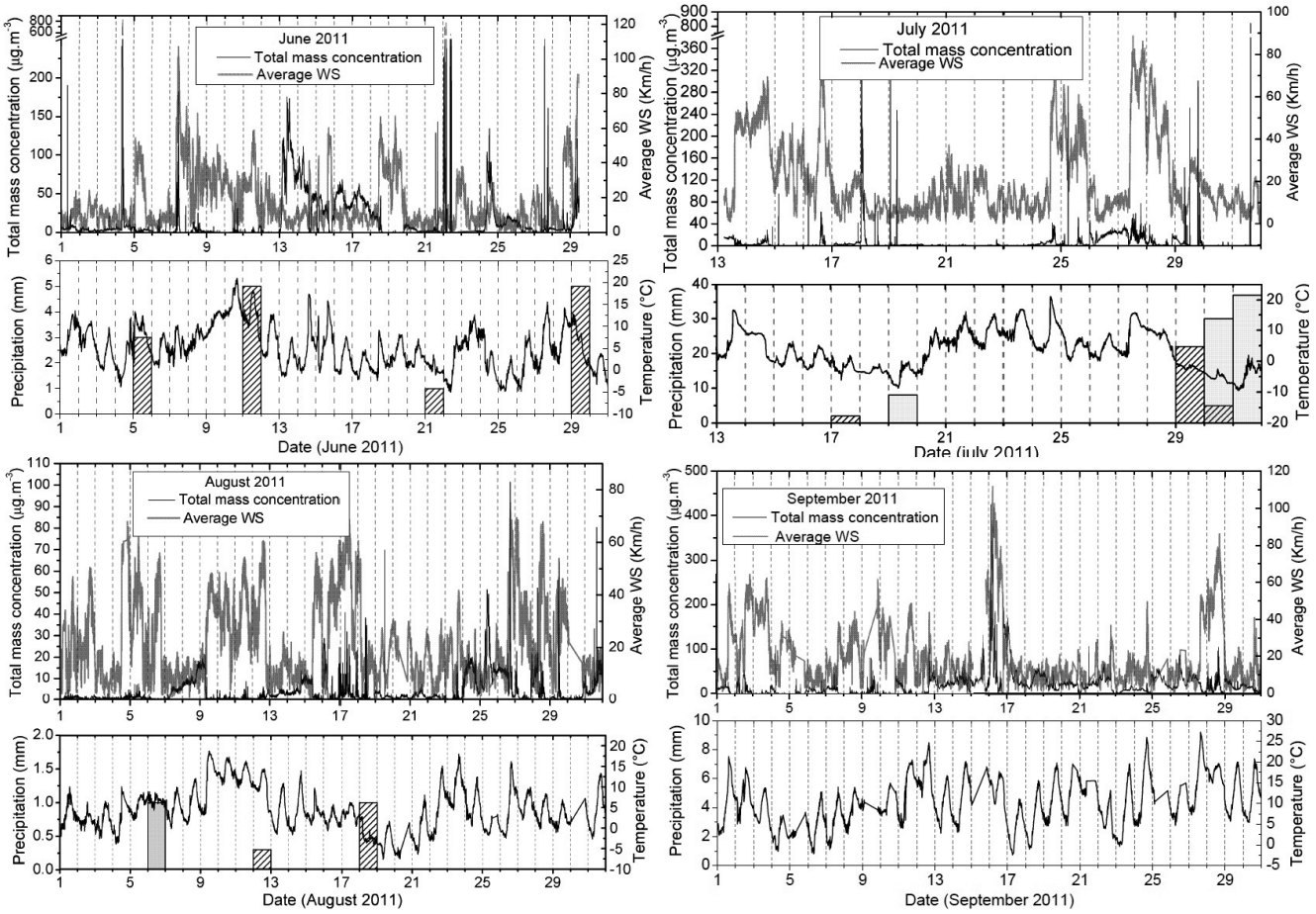


**Fig. 7.** Aerosol total mass concentrations and local meteorological variables at ground as a function of time. For each month, upper panel: concentration and wind speed (WS) and lower panel: precipitation (rain: striped bars of a daily basis histogram, snow: shaded bars) and temperature.

On the other hand, the July low mean concentration value can be indeed attributed to low temperatures, as this is in fact the coldest winter month while, instead, its continentality value and aerosol size distribution pattern are similar to June and September. This fact indicates that the atmospheric conditions on July 2011 were clearer, not for having more proportion of air masses carrying sea aerosols from the ocean but for the lower amount of suspended soil aerosols due to low temperatures (even when the coarse fraction characteristic of dust is still clearly dominant and its contribution to the total concentration is comparable with that found during hazier months like June and September). It can be noted that the lower standard deviation values of the mean continentality ($\langle C \rangle$) for the hazy conditions with respect to the clear ones for all the PM analysed, seems to indicate that the hazy situation has a more definite origin, related with the Andean dust, while the clear situation can have a more variable origin (as explained for the July and August cases).

The sudden increase in aerosol mass concentration from August to September 2011 found for the data registered with the Grimm aerosol spectrometer 1.109 (see table 1) is in accordance with the pronounced increase found for the same seasonal period with a nine years dataset of CLF measurements (from January 2004 to December 2012) [8]. It is also in agreement with a similar trend found for this period for aerosol mass concentrations obtained by gravimetric analysis of aerosol samples collected in filters during 2008 [3].

### 3.2 Effect of local meteorological variables

To investigate the validity of the approach of sect. 3.1 based on the study of correlations between air mass trajectories and local aerosol data, the effect of local meterological variables at the ground level during the measurement period was considered.

Figure 7 presents the aerosol mass concentration registered by the Grimm 1.109 aerosol spectrometer, as a function of time, for all months as in fig. 1(a), with the addition of wind speed (upper panel) as well as precipitation and temperature (lower panel). The local wind speed and temperature values are supplied by a weather station placed on

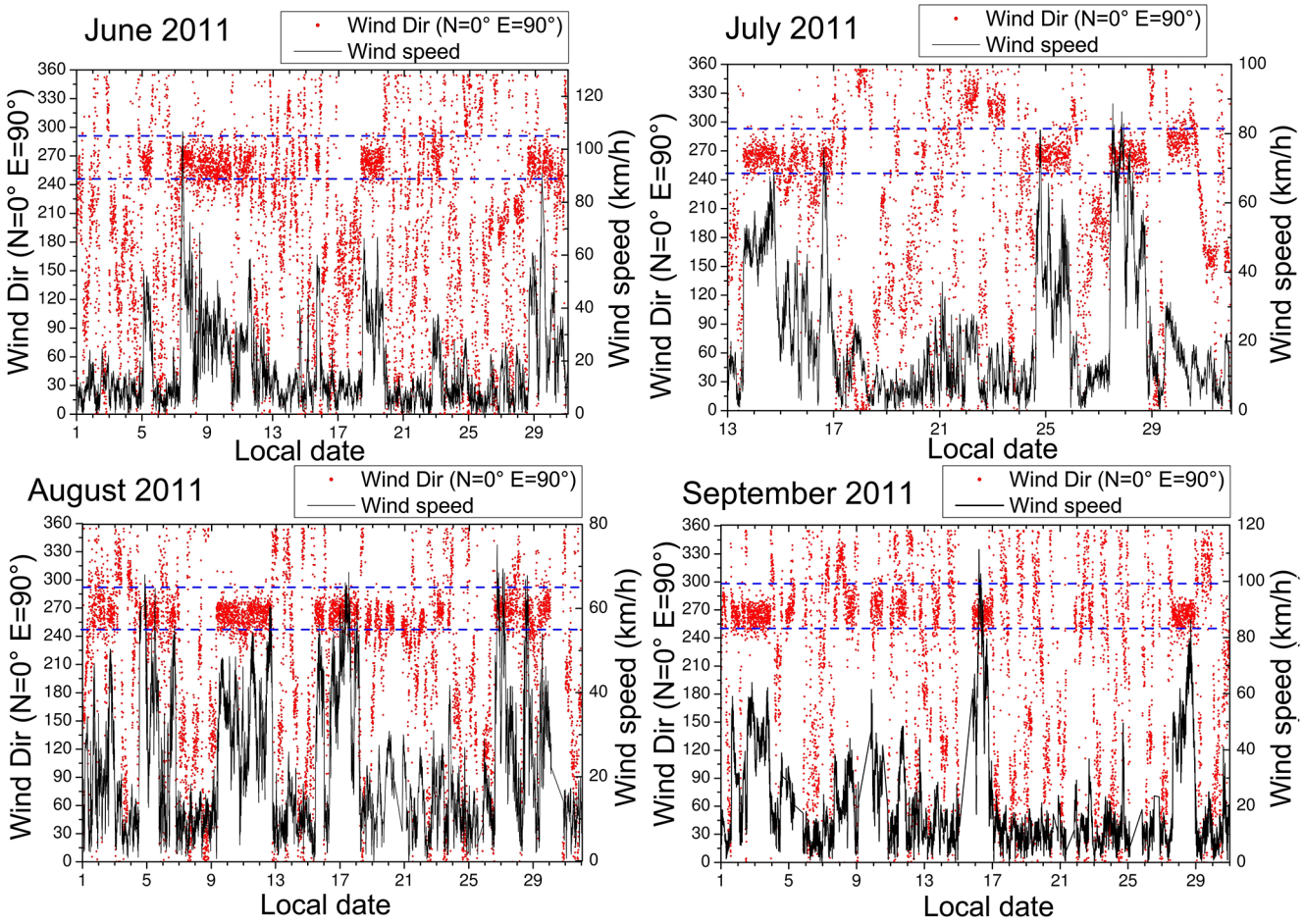


**Fig. 8.** Local wind arrival direction (red points) and wind speed (grey continuous line) as a function of time, for the winter months of 2011, registered by the P. Auger Observatory weather station at Coihueco FD building. The blue dashed lines enclose the W direction: ($270° \pm 22.5°$). The wind directions corresponding to peaks of high wind speeds, fall in this W band.

the roof (at about 6 m AGL) of the FD building at Coihueco (35° 06′ 50.52″ S, 69° 35′ 59.33″ W, 1690 m ASL) (one of the five weather stations of the P. Auger Observatory, that records data every 5 minutes [2]), the same site at which the aerosol concentration values are registered with the Grimm 1.109 instrument. The precipitation (rain and snow) data are provided from the weather station from the Argentinean National Meteorological Service (international number: 87506) at Malargüe Aerodrome (35° 30′ S, 69° 35′ W, 1426 m ASL). The distance between both weather stations is of $\sim 40$ km.

The tall and sudden peaks in concentration occur in a very short temporal period (they can last 5 or 15 minutes, for example), not appreciably contributing to the mean values of each month. They can be attributed to local singularities of unknown and random origin (like gusts or dust whirlwinds limited to a very small spatial scale or the eventual arrival of a vehicle from the Pierre Auger Observatory to the measurement site). These singularities can be easily detected from the normal behavior of concentration, so they cannot be considered as representative of the situation of aerosols at the atmosphere but only of a particular micro-event with influence at the air flow entrance of the Grimm 1.109 device. As can be observed in fig. 7 the aerosol total mass concentration (upper panel) tends to decrease after precipitation (rain or snow) events, in which a decrease in temperature also takes place. On the other hand, there is not a clear correlation between an increase in wind speed and in concentration, apart from few cases —specially when the wind peak is wide enough in time and tall (about 100 km/h) like the peak of 15–17 September.

Wind direction data —also supplied by the P. Auger Observatory weather station at the roof of Coihueco FD building where aerosol concentrations and wind speeds are measured— are correlated with wind speed data. This correlation as a function of time is shown in fig. 8 for each month. Every peak of high wind speed (reaching approximately 60 km/h or more) corresponds to winds overwhelmingly arriving from the West direction, defined as in sect. 3.1 by the angular range ($270° \pm 22.5°$) denoted between dashed lines in the figure (angular directions increase in clockwise direction, starting at North with 0°). The red points (corresponding to wind direction data) are highly concentrated in the West ($270° \pm 22.5°$) band during wind speed peak events (wind speeds are denoted by gray continue lines).

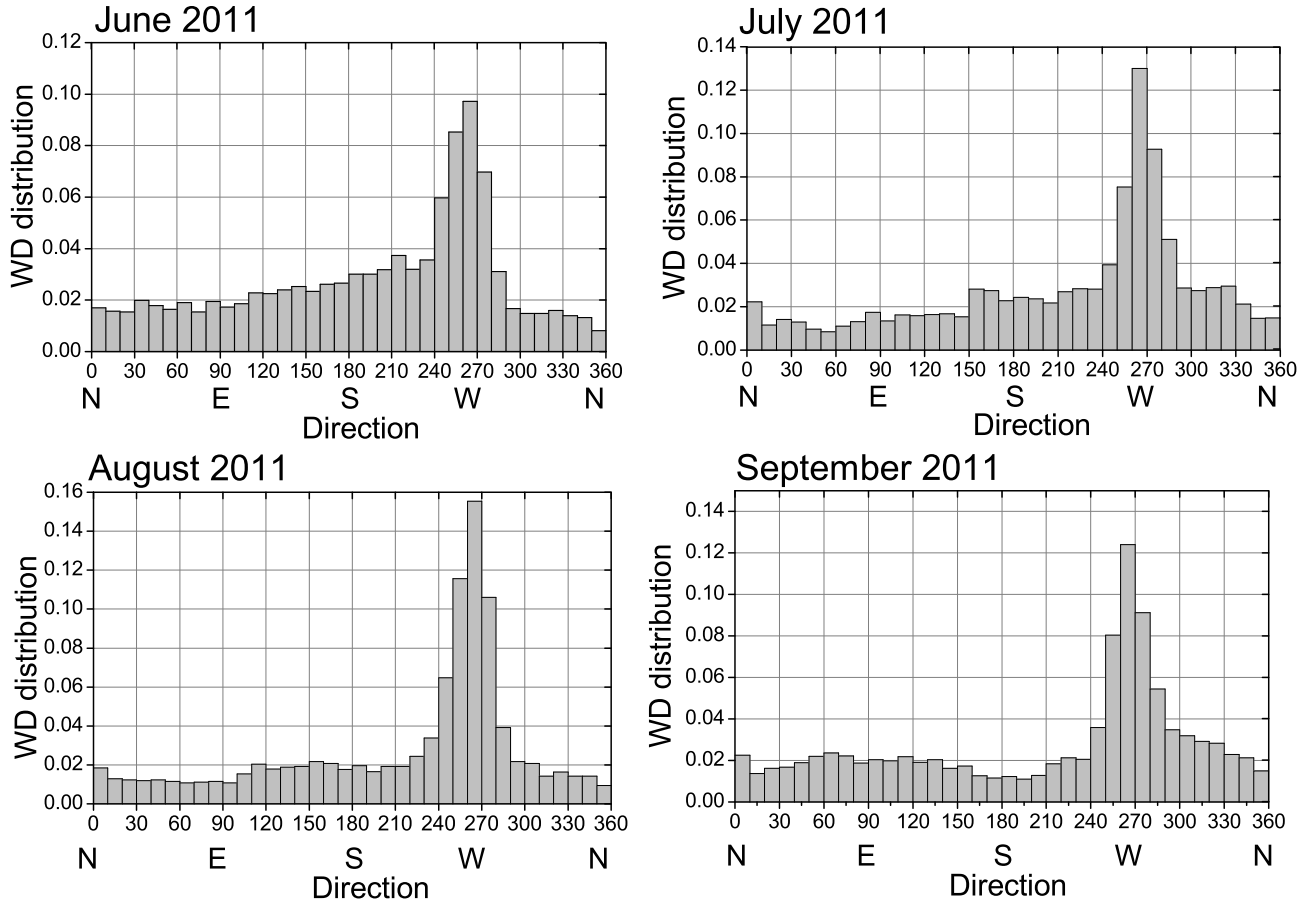


**Fig. 9.** Histogram of the local wind direction distribution at Coihueco for the winter period corresponding to Grimm 1.109 aerosol concentration measurements (for July, from 14 July to the end of month).

Other cardinal arrival directions are related with lower wind speeds. The fact that higher values of wind speed are associated with westerly winds, can be responsible for the weak or negligible effect of an increase in aerosol concentrations with higher wind speeds. Even more, high speeds of winds are frequently associated with a decrease in aerosol concentration in fig. 7. In fact, westerly winds arrive from the Pacific ocean and have lower continentality values, thus carrying a lesser content of dust from the desert Andean region, lifted and blown through their passage, in comparison to winds from other cardinal directions. So, local wind velocity analysis does not alter the main conclusion of the previous section, concerning the principal effect of continentality values, as obtained by means of HYSPLIT trajectories, in determining the clean/dirty situation at this typical site at the desert-like Andean region in Argentina. As can be observed in fig. 8, August 2011 is the month more influenced by high-speed westerly winds.

The local wind direction distribution at Coihueco for each winter month of 2011 is depicted in fig. 9. The dominant wind arrival direction is from the West, specially in the angular interval between 260° and 270° for every month, but in a more pronounced way for August. June presents a significant contribution of winds from the South (in the range 90°–270°, mainly SW: 180°–270°), while September, from the North (range 0°–90° and specially NW: 270°–360°). A similar analysis but in polar coordinates is represented in fig. 10, also showing the same features for wind direction distribution as described above, particularly, the well-defined West direction for the arrival of winds during August, in accordance with the air mass analysis made by using HYSPLIT and with the lower continentality value for this month, as discussed in the previous section.

Special attention was paid in the analysis of the peaks of aerosol concentration found for June because for some days a correlation was found between those peaks of high concentration and air masses coming from the area of the Chilean Volcano Puyehue (40° 34′ 59.88″ S, 72° 7′ 59.88″ W), which begun an eruption process on June 4th, 2011, with an eruptive column of 10 km height, spreading ashes on large regions of Argentina. The eruption was more intense in June but lasted several months including the whole period analysed in this work. For this reason, the period of winter studied here was investigated in connection with the possible arrival of air masses from the volcano and only for June such air masses were found to actually reach the site of the P. Auger Observatory. As most winds flow in the Andean region in the eastward direction, the ashes easily reached the eastern Argentinean areas (including Buenos Aires) but

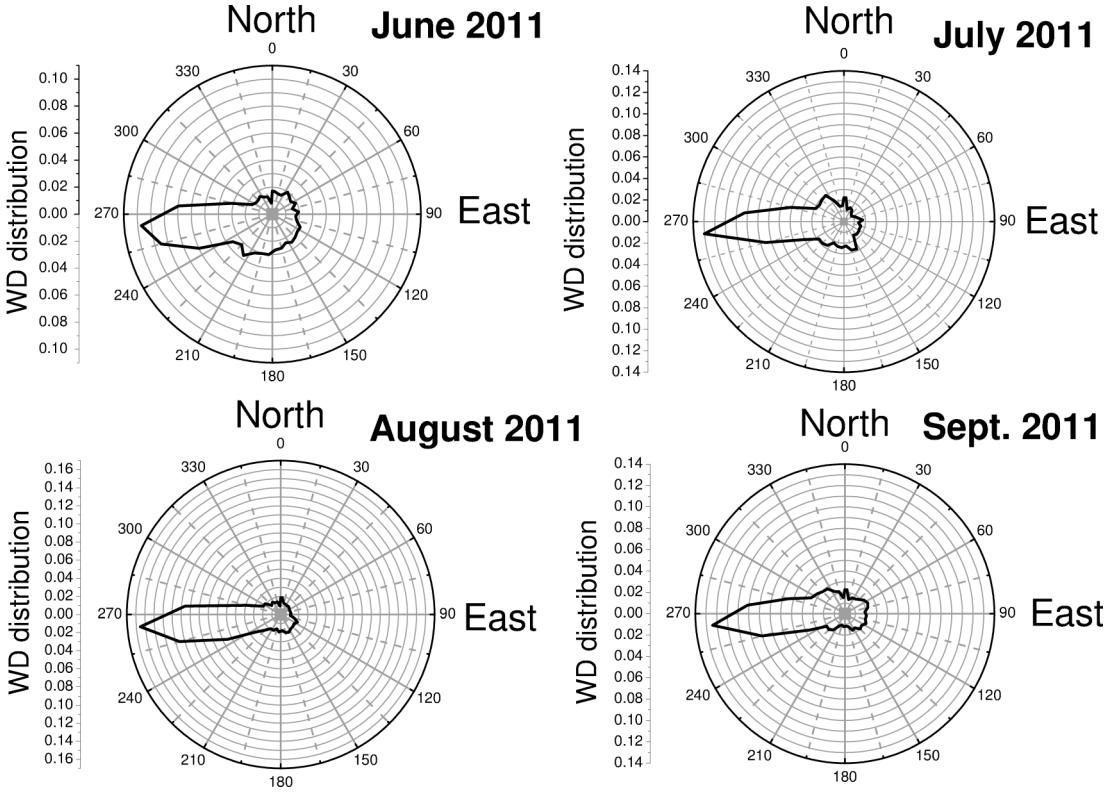


**Fig. 10.** Polar diagrams of wind direction distribution (probability density function of local wind arrival directions at Coihueco) for the winter period corresponding to Grimm 1.109 aerosol concentration measurements (for July, from 14 July to the end of month). The scale on the left side of each polar diagram is the radial one. The length of the radial coordinate indicates the probability for a given direction and the angular coordinate the direction itself (with angular intervals of 10°).

they hardly travelled in the northward direction, along the Andean mountains, so their effect on our measurement site at the P. Auger Observatory was not significant, except for some special days of June. In fact, when observing figs. 9 and 10 we note that June 2011 presents a higher proportion of winds reaching the P. Auger Observatory from the SW direction (where the volcano is placed) than the other months. By means of a detailed study of HYSPLIT backtrajectories and satellite data we found correlations between winds from Puyehue and high concentrations for the events of 7 June and 13 June and the next days. Images of MODIS (Moderate Resolution Imaging Spectroradiometer) instruments (on board of TERRA and AQUA satellites, NASA) show the eruptive plume departing from the volcano in northward direction for the days 6 June and 12 June, reaching the zone of the P. Auger Observatory in correspondence with the high aerosol concentration values detected by the Grimm 1.109 on 7 June and 13 June and the next days. A grey haze suspended in the atmosphere at the site of the P. Auger Observatory was reported on June 7th by P. Auger Collaboration members as local observers [15]. It is important to note that the effect of the volcano eruption for this particular period is not affecting the correlations found in this work for continentality and aerosol behaviour, as the ashes arriving from volcano are due to a higher continentality value in June with respect to August and to a higher proportion of air masses arriving at the P. Auger Observatory from the South as can be observed in fig. 3. This figure shows a higher density of HYSPLIT trajectories from the region of the Puyehue volcano for June than for the rest of the period. This confirms the good correlation found between HYSPLIT air mass trajectories and aerosol concentrations measured locally at ground level and the importance of the air mass trajectory tool when local data are not available. The effect of volcano Puyehue during June 2011 can be noted in the higher aerosol mean mass concentration value obtained at Coihueco site during June in 2011 in comparison with the same month of a previous year [3] and in the important proportion of coarse particles according to fig. 2 and table 1 (June is the month with the highest percentage of particles in the coarse range $PM_{2.5\text{-}10}$ during the analysed period).

Comparison between the results of HYSPLIT trajectories and satellite data, and wind directions locally registered at the Coihueco weather station was performed for these special ashes events during June 2011. Figure 11 shows that around the peak of concentration events of 7 June and 13 June, most of the local winds arrived from the Southern hemisphere of a polar diagram centered in Coihueco (angles between 90° and 270°), carrying the ashes that arrive directly from the volcano plume (from the SW direction) or the ones previously spread in eastern zones of Patagonia (South to the Auger Observatory).

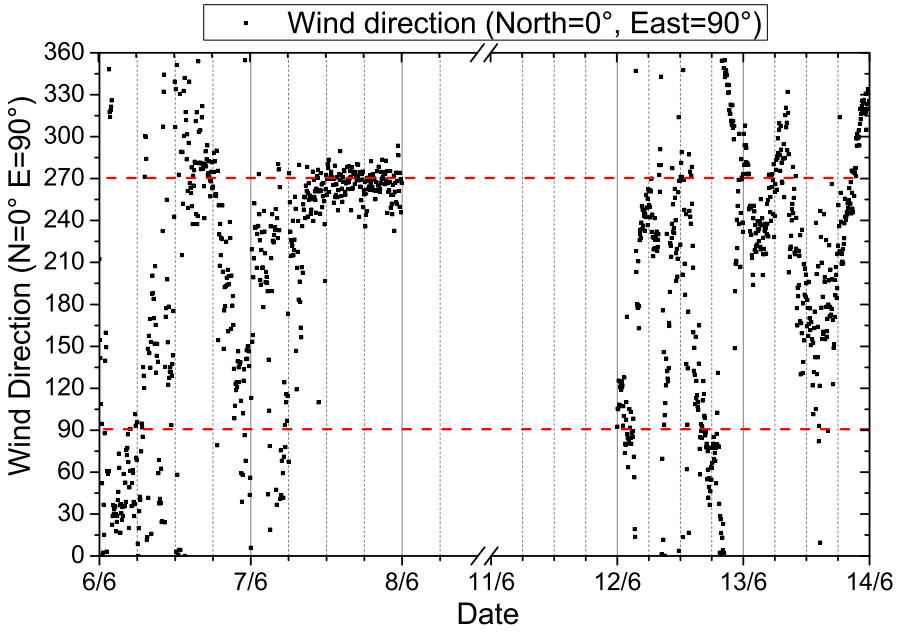


**Fig. 11.** Local wind direction measured in Coihueco for the days of events correlated with the arrival of ashes from volcano Puyehue, during June 2011. The red dashed lines enclose a band that corresponds to the Southern hemisphere in a polar diagram centered in Coihueco. Most of the winds at Coihueco arrive from the S during those days.

The effect of volcano ashes makes June 2011 a month with a mean mass $PM_{tot}$ value anomalous high for this cold winter month and similar (see table 1) to the one obtained for September (late winter and beginning of spring, with appreciably higher temperatures, where a peak in the aerosol content has been reported for different years as registered by different devices of the P. Auger Observatory [3,8,11]). Figure 1(a) shows that, apart from the tall and short period peaks with no significant contribution in the mean monthly values, September presents higher aerosol mass concentrations $PM_{tot}$ in a more regular way throughout the month than June. The latter has very low concentrations for most of its period, being the peak between 13th and 19th the major responsible for the high mean mass $PM_{tot}$ for June. Figure 8 shows between those days a high proportion of low-speed winds from the South, thus carrying the volcano ashes (directly from the volcano plume or previously spread over Patagonia region). Figure 7 (that shows that no precipitation events occur during the peak of concentration of 13–19 June) and fig. 8 (with low-speed winds blowing mostly from South directions for this period) indicate that these ashes have been suspended in the sky over the P. Auger Observatory until high-speed winds from the West begun to blow at the end of 18 June and continued blowing during the next days, cleaning the atmosphere.

To the effect of the ashes originated in the Puyehue volcano eruption and carried by southerly winds to the P. Auger Observatory, on the higher mass concentration values registered for June 2011 in comparison with June of previous years [3] and with other winter months (July and August 2011) of comparable lower temperatures, can be added the fact that June 2011 did not present snow events. The effect of the snow in cleaning the atmosphere should be considered not only as a local one (by maintaining the local dust under the snowy layer) but also at a larger scale, as the snow distributed over the Andean areas during winter prevents winds crossing those areas from becoming "dirty" by lifting the dust of this desert-type region. The combined effect of the absence of snow and rain and, specially, the volcano emissions, made June 2011 almost as dirty as September 2011 (see mass concentrations $PM_{tot}$ in table 1).

The mean temperatures for each month of winter 2011 of table 3, obtained from data registered at Coihueco (in the countryside region and on a hill at 1690 m ASL) are somewhat lower than the ones registered at the Aerodrome of Malargüe (between 6 a.m. and 9 p.m., in a flat area at 1426 m ASL) presented in sect. 3.1. It is interesting to note that the mean temperatures show a better correlation with the mean particle concentration $PM_{tot}$ than with the mean mass concentration $PM_{tot}$. In fact, July is the coldest month and the one with the lowest mean particle concentration $PM_{tot}$ but August presents the lowest mean mass concentration, as given by table 1. June and August have similar mean temperature values and similar mean particle concentrations. Instead, they greatly differ in mass concentration, being June a much "dirtier" month than August, since suspended particles in June are much bigger than in August (as shown in fig. 2) leading to an appreciable higher amount of suspended aerosol mass in June in comparison with August. We can conclude that temperature correlates with particle concentration, in the sense that low temperatures are connected with low particle $PM_{tot}$, attributed to the effect of snow and frost in keeping aerosols captured on ground and on the lower air convection caused by heat that raises air with the dust of the ground. On the other hand, continentality values and air mass trajectory analysis correlate with aerosol mass concentration and size distribution,

**Table 3.** Mean montly values and standard deviations for temperature, wind speed and wind direction (Coihueco weather station). In case of the mean monthly value of precipitation (Malargüe Aerodrome weather station), a distinction is made between rain and snow in the format: rain (snow). N means that there is not precipitation recorded for the period. For July, the mean values of the meteorological variables are calculated only over a period of 18 days corresponding to the concentration measurements with Grimm 1.109 (from 14 to the end of month), except for precipitation where the mean over the whole month was also included (second option in the table) (there was not precipitation before 14 July).

| Month (2011) | | Air T (°C) | WS (km/h) | W Dir (N = 0° E = 90°) | Prec. Rain (Snow) (mm/day) |
|---|---|---|---|---|---|
| June | mean | 5.1 | 16.9 | 198.8 | 0.47 (N) |
| | std dev | 4.9 | 15.1 | 87.8 | |
| July | mean | 3.3 | 20.9 | 218.0 | 1.61 (3.72)/0.94 (2.42) |
| | std dev | 6.2 | 18.4 | 88.1 | |
| August | mean | 4.5 | 21.7 | 217.8 | 0.04 (0.03) |
| | std dev | 5.2 | 15.5 | 84.0 | |
| September | mean | 10.1 | 20.2 | 211.1 | N (N) |
| | std dev | 5.8 | 17.4 | 97.4 | |

as explained in sect. 3.1. These correlations are found for the first time in this work for the P. Auger Observatory, clarifying the origin and characteristics of the aerosols present in it, thus allowing one to choose between different types of aerosols in radiative transfer programs that take into account the attenuation of the fluorescence light caused by cosmic ray showers in the atmosphere. These correlations can be extended also to other similar Andean sites of astronomical/astrophysical/solar interest.

The analysis introduced in sect. 3.1 can be considered as a "general" one, as it is based in the calculation of the mean values of different parameters (concentration, continentality, wind direction) for different situations (size range, "clean" or "dirty" atmosphere). With this approach based in mean values we obtained the main results stated in sect. 3.1, which is the "key" section of this work as it shows the correlation between aerosol concentration measurements and air mass trajectories at the Pierre Auger Observatory. On the other hand, sect. 3.2 consists of a detailed analysis of the effect of local meteorological variables at ground level in aerosol concentration data, for every day of measurement. In this sense, it can be considered as a "particular" analysis, as it takes into account the correlations between every day measurement of aerosol concentration and meteorological data, including the specific events.

It is worth pointing out that the general analysis of sect. 3.1 by using air mass trajectories and the continentality parameter presented in this work is previous to the particular event study and correlation with local meteorological parameters, which confirmed *a posteriori* the validity of the conclusions obtained from 1.3. Even when an abrupt and non-frequent event as a volcano eruption could happen, as in June 2011, the validity of the air mass analysis and of the use of the continentality parameter remains. In fact, the HYSPLIT trajectories during the volcano eruption, helped in the understanding of the peaks of aerosol concentration found during June 2011 at the P. Auger Observatory and of the differences with respect to June of other years. Satellite data and an analysis based on meteorological local variables confirmed the results (for example, fig. 11 shows the local southerly winds related to peaks of concentrations at the P. Auger Observatory, during the volcano event).

Summarizing the effect of meteorological variables, it can be stated that temperature and precipitations have a local influence in aerosol conditions, mostly in aerosol particle concentration, related to their effect in washing the atmosphere (by rain and snow) and in keeping the aerosols at ground (when low temperatures are responsible of frost and of layers of snow that remain covering the soil during some period of time). But they also have a regional effect linked to maintaining this kind of conditions along the region traversed by the winds during the cold weather an precipitation periods. HYSPLIT air masses trajectories can shed light on this regional effect, by knowing the areas traversed by winds and the conditions of temperature and precipitations in them. By using data of these meteorological variables obtained from weather data bases (like the one of the Argentinean National Meteorological Service) combined with air mass trajectories, one can perform an adequate estimation of the aerosol situation at Andean regions like the one of the P. Auger Observatory or similar ones (where antropogenic aerosols sources are scarce in comparison with natural ones). About local meteorological variables related with wind, like wind direction and wind speed, they showed to match the same conclusions that were previously deduced by using HYSPLIT air mass trajectories for this Andean region sites. Wind direction (from Ocean or from continental areas) was found to be determinant in the general aerosol situation. Wind speeds are related with wind directions (higher speeds for winds from the West). We can conclude that in general, high-speed westerly winds are a dominant cause for the cleansing of the atmosphere at the P. Auger Observatory location. Wind and air mass trajectories mostly influence the aerosol size distribution pattern

(depending on the sources: the Pacific Ocean, the Andean dust or an eventual special one like a volcanic eruption, for example) and, consequently, the aerosol mass concentration values. In this way, sect. 3.2, looking also at meteorological parameters at ground, validated the general analysis of sect. 3.1 and helped in the understanding of how the aerosols at the P. Auger Observatory or similar conditions Andean sites, are influenced by long-range transportation and local variables. The good agreement found between both approaches can be considered as a significant result to be employed in Andean similar places where local aerosol measurements are not available.

## 4 Conclusions

- Aerosol concentration measurements at the Pierre Auger Observatory of cosmic rays, at the Andean region in Argentina, were correlated with HYSPLIT air mass trajectories arriving at this site, confirming that these trajectories are a useful tool for understanding the aerosols at this site as was shown by a previous analysis of correlations between VAOD measured at the observatory and air mass displacements [7].
- The present study incorporates data on mass and particle concentration at surface level for different size ranges, provided by the Grimm 1.109 instrument. The size distribution analysis in correlation with air mass behaviours provides a more complete insight into the origin and evolution of aerosols at the site. A size analysis in relationship with sources and displacement of aerosols was not possible with the VAOD measurements [7] and turns out to be of significant interest for the understanding of the aerosol conditions.
- This work shows for the first time measurements of size distribution of aerosols at the Pierre Auger Observatory and is a pioneer for this kind of astrophysical facilities. Aerosol size plays a role in the light transfer process in the atmosphere, taken into account in cosmic ray shower reconstruction. Also the type of the aerosols (that determine their scattering or absorbing properties) enter in those calculations. So, the improvement of the knowledge of the origin (sources) and evolution of aerosols is important for this purpose. But it is also of major importance in many other fields (atmospheric sciences, human health, ecosystem studies, etc.) in which these atmospheric particles play a significant role. Thus, the results are applicable also to these fields.
- Thanks to the size distribution analysis, a distinction between cases of comparable low aerosol mass concentration is possible. This is the case for July and August 2011, that nevertheless significantly differ in the size distribution pattern which gives information about particle sources. August, the month with less proportion of time of travel of the air mass trajectories over continental areas (as given by a parameter, named continentality, defined in this work) is the one with the clearest atmospheric conditions and with the highest proportion of fine aerosols. The size distribution of August differs from that of the rest of the analysed winter period. The lower continentality value and the higher proportion of lighter particles indicate that during August 2011 the atmosphere over the Pierre Auger Observatory was appreciably influenced by marine aerosols. Instead, July presents similar continentality value and size distribution pattern to the rest of the period (except August), with the predominance of coarse particles, which correspond to the Andean dust. Its low mean total mass concentration value is then attributed to the lowest temperatures of the winter present during this month, maintaining the snow and frost covering an important amount of soil particles. Thus, low ambient temperatures can be responsible for low mass concentrations but the link between time over continental areas and mass concentration is found to be stronger in defining the clear/dusty atmospheric situations at the studied site and responsible for the aerosol size distribution pattern.
- A parameter named "continentality" defined as the percentage of time in which an air mass trajectory traverses land areas with respect to its total traveling time (over land and sea), territories as well as its mean value for different situations, was introduced in this work, showing to be suitable for interpreting and quantifying the correlations found between the air mass trajectories paths and the aerosol mean mass and particle distributions.
- A correlation was shown between higher continentality values and hazier conditions. This tendency is more pronounced for the coarse fraction $PM_{2.5\text{-}10}$ of $PM_{10}$, as most of the particles of this range consists of suspended dust of the desert Andean region (coming from the N or NE directions). On the other hand, the results indicate that the fine $PM_{2.5}$ fraction could be caused either by sea aerosols (coming from the NW) of from anthropogenic ones (from the N or NE).
- The size distribution characteristics of the aerosols sampled at ground are in accordance with the ones of the aerosols generated by the sources pointed by the air mass backtrajectories, transported by winds over a 48 h or 24 h time interval, and arriving into the boundary layer over the measurement site.
- The approach presented in sect. 3.1, based on the correlations between aerosol mass and particle distributions, and air mass trajectories, by analysing the mean values of different parameters, including the continentality one introduced in this section, is complemented and validated in sect. 3.2 by a detailed analysis of the effect of local meteorological variables at ground level on the aerosol concentration measurements. This complementary approach helps in the understanding of the link between long-range transported aerosols and those locally characterized.

- The inclusion of local observables like the meteorological variables at the measurement site, including also the topographic profiles at the site and its surroundings, as well as an evaluation of the influence of anthropogenic aerosols from cities placed in the region crossed by the air mass trajectories, clarifies the panorama of the aerosol situation at the Pierre Auger Observatory.
- This study was possible thanks to the vast atmospheric monitoring network at the Pierre Auger Observatory —that includes weather stations at the aerosol sampling location— making it a unique and privileged site for atmospheric studies in the Andean Argentinean region. Interdisciplinary studies at this observatory are encouraged by the Auger Collaboration [6].
- Once a correlation has been found between air mass trajectories (arrival directions, time over continental areas, sources at which the trajectories point) and local measurements of aerosol size distribution patterns, as in the present work, the HYSPLIT model offers the possibility of inferring the aerosol characteristics independently of an instrumental setup and a permanent data taking process, which is not always feasible.
- The applications of the work exceed the local interest at the Pierre Auger Observatory, as they can be extended to other Andean regions of Argentina with similar characteristics in topography, winds, density of population, sources of aerosols, etc., where there is a lack of local measurements (due to the vast range of the Andean zone, the absence of local instruments, the difficult logistics for data-taking campaigns due to the isolated mountain areas). In these situations, the link found between air mass trajectories and aerosol concentration (total and as size distribution) in the present work, could help in inferring aerosols origin and characteristics by using HYSPLIT trajectories in the mentioned areas. This is supported by a recent study that compared aerosol concentration measurements performed with the same Grimm 1.109 instrument at the Auger Observatory and at other Andean sites proposed for the construction of big astronomical/astrophysical/solar facilities, showing that these sites have similar conditions of low aerosol content [14]. Different air mass behaviours at these Andean places can be connected, as a first approximation, with the different aerosol scenarios found in the present study when local measurements are not available for a given site and time. This knowledge is specially valuable at present due to the fact that the Andean Argentinean region is increasing its status as a good candidate to host big facilities like astronomical and astrophysical observatories and solar centrals [14].

MIM and RDP acknowledge the economic support of CONICET and ANPCyT. KL thanks Dr. Marcel Urban for having been at the beginning of this study. Also, MIM, KL and PV thank their colleagues from the Pierre Auger Collaboration for fruitful discussions about this work. Discussions with Engineer Gualberto Ávila concerning the experimental setup were considerably valuable. The authors express their gratitude to Leandro Gómez for the technical support he provided during the installation and operation of the Grimm 1.109 aerosol spectrometer at the Pierre Auger Observatory, and to the Pierre Auger Collaboration members that are responsible for the weather stations data of the observatory.

## References

1. A. Aab *et al.*, Nucl. Instrum. Methods Phys. Res. A **798**, 172 (2015).
2. J. Abraham *et al.*, Astropart. Phys. **33**, 108 (2010).
3. M.I. Micheletti, L.G. Murruni, M.E. Debray, M. Rosenbusch, M. Graf, G. Ávila Cadena, P. Vitale, J. Davidson, H. Somacal, Nucl. Instrum. Methods Phys. Res. B **288**, 10 (2012).
4. R.R. Draxler, G.D. Rolph, *HYSPLIT (HYbrid Single-Particle Lagrangian Integrated Trajectory)*, Model access via NOAA ARL READY website, `http://www.arl.noaa.gov/HYSPLIT.php`, NOAA Air Resources Laboratory, College Park, MD (2013).
5. G.D. Rolph, *Real-time Environmental Applications and Display sYstem (READY)*, `http://www.ready.arl.noaa.gov`, NOAA Air Resources Laboratory, College Park, MD (2013).
6. K. Louedec, Pierre Auger Collaboration, R. Losno, Eur. Phys. J. Plus **127**, 97 (2012).
7. K. Louedec, Pierre Auger Collaboration, J. Phys.: Conf. Ser. **409**, 012236 (2013).
8. A. Aab *et al.*, Atmos. Res. **149**, 120 (2014).
9. NOAA Air Resources Laboratory (ARL), *Global Data Assimilation System (GDAS1) archive information*, tech. report, `http://ready.arl.noaa.gov/gdas1.php` (2004).
10. P. Abreu *et al.*, Astropart. Phys. **35**, 591 (2012).
11. V. Rizi, A. Tonachini, Pierre Auger Collaboration, M. Iarlori, G. Visconti, Eur. Phys. J. Plus **127**, 92 (2012).
12. J.N. Porter, A.D. Clarke, J. Geophys. Res. **102**, 6035 (1997).
13. D. Morata, M. Polvé, A. Valdés, M. Belmar, M.I. Dinator, M. Silva, M.A. Leiva, T. Aigouy, J.R. Morales, Environ. Geol. **56**, 81 (2008).
14. R.D. Piacentini, B. García, M.I. Micheletti, G. Salum, M. Freire, J. Maya, A. Mancilla, E. Crinó, D. Mandat, M. Pech, T. Bulik, Adv. Space Res. **57**, 2559 (2016).
15. Martin Will, private communication.